Nguyen Khac, Hoang; Modabberian, Amin; Zenger, Kai; Lendormy, Éric; Mikulski, Maciej; Hunicz, Jacek

A Neural Network Approach for Reconstructing In-Cylinder Pressure from Engine Vibration Data

Published in:
SAE Technical Papers

DOI:
10.4271/2022-01-1038

Published: 30/08/2022

Document Version
Peer-reviewed accepted author manuscript, also known as Final accepted manuscript or Post-print

2022-01-1038

A Neural Network Approach for Reconstructing In-cylinder Pressure from Engine Vibration Data

Hoang Khac Nguyen, Amin Modabberian, Kai Zenger
Aalto University

Éric Lendormy
Marine Solution Engines, Wärtsilä

Maciej Mikulski
University of Vaasa

Jacek Hunicz
Lublin University of Technology

Abstract

In this work neural network models are used to reconstruct in-cylinder pressure from a vibration signal measured from the engine surface by a low-cost accelerometer. Using accelerometers to capture engine combustion is a cost-effective approach due to their low price and flexibility. The paper describes a virtual sensor that re-constructs the in-cylinder pressure and some of its key parameters by using the engine vibration data as input. The vibration and cylinder pressure data have been processed before the neural network model training. Additionally, the correlation between the vibration and in-cylinder pressure data is analyzed to show that the vibration signal is a good input to model the cylinder pressure.The approach is validated on a RON95 single cylinder research engine realizing homogeneous charge compression ignition (HCCI). The experimental matrix covers multiple load/rpm steady-state operating points with different start of injection and lambda setpoints. A radial basis function (RBF) neural network model was first trained with a series of two operating points at low loads with data of 1000 consecutive combustion cycles, to build the needed nonlinear mapping. The results show that the developed neural network model is capable of reconstructing in-cylinder pressure at low loads with good accuracy. The error for combustion parameter such as maximum cylinder pressure did not exceed 5%. The approach is further validated with another series of operating points consisting of both low loads and high loads. However, the results in this case deteriorated. Changing the neural network model to generalized regression (GR) improved the in-cylinder pressure reconstruction quality. The performance of the models was also considered in terms of combustion parameters, such as maximum pressure and mass burned fraction. The paper concludes that vibration signal carries sufficient information to estimate combustion parameters independently on the engine platform or combustion concept.

INTRODUCTION

Demands for emission reduction and efficiency improvement in internal combustion engines are increasing everyday, and therefore, novel combustion concepts and highly optimized controllers are developed. In the combustion process specifically the cylinder pressure is a vital component, which can be utilized for the optimization of the engine performance, emission reduction and even fault detection (misfire, knock detection) [1–6].

The standard method for cylinder pressure measurement is by using transducer inserted into the cylinder head of the engine. This method is expensive and not reliable in long term due to the limited lifetime of the transducers being exposed to severe conditions (high temperature, high pressure). Therefore, many different non-intrusive or indirect methods to acquire the combustion data have been developed, which mainly rely on vibration measurements [7–11]. In addition, simple optical methods [12] and ionisation measurement techniques [13, 14] are also being investigated. There is a strong correlation between the cylinder pressure and the vibration of the engine because the fast changing in pressure during combustion causes the vibration on the engine block [15, 16]. The cited research indicates that vibration data contains important information about the cylinder pressure. Hence, there are possibilities of reconstructing the cylinder pressure from the vibration on the engine block. Vibration signal is easily measured from accelerometers attached on top of the cylinder head or on the frame of the test bench. However, there are some difficulties, because the cylinder pressure is not the only source of the vibration. The non-linear correlation between the pressure and the vibration makes the function approximation process difficult [17].

Recently, many researchers have taken different approaches to estimate the pressure curve from the accelerometer signal, applied on both spark ignition and compression ignition engines. In [8] and [9], a recursive method using Kalman filter has been proposed. Frequency-based coherence analysis methods were used in [18] and [19] to estimate combustion parameters from accelerometer signal. Artificial neural networks have also been proven to be a reliable method in [17], [20], [21]. In these works, radial basis function neural network, recurrent and generalized regression network were implemented to reconstruct the cylinder pressure of diesel engine and gas engine with good results. However, there is very little work related to homogeneous charge compression ignition (HCCI) engines. Results in [22] and [23] show that generalized regression neural networks can be good tools for combustion parameter estimation for HCCI engines.

In this paper, an approach using radial basis network models is proposed to reconstruct engine cylinder pressure from accelerometer signal. The models were trained with data from an HCCI engine and the validation of the predicted results are also presented. Error of the validation is analyzed in terms of combustion parameters such as peak pressure and 50 % mass fraction burned.

EXPERIMENTAL SETUP

Experimental data in this work has been collected from a single-cylinder HCCI engine test bench at Lublin University of Technology. Detailed specification of the engine is presented in Table 1. Figure 1 shows the cross-section view of the engine. The engine's head uses hydraulic mechanism to reduce valve lifts and enables negative valve overlap operation [24]. Notably, this mechanism is responsible for high valve opening and closing noise. Cylinder pressure is measured by a GH12D miniature pressure transducer. The transducer is mounted on the engine head and connected via a charge amplifier to the test bench acquisition system. An optical encoder with a 0.1 crank angle degree (CAD) resolution triggers the high-speed pressure data. Vibration signal is measured by accelerometers attached on the upper surface and side surface of the cylinder head, as shown in Figure 2. The vibration signal is also sampled with corresponding resolution of 0.1 CAD. Table 2 shows the accelerometers specifications. The engine was coupled to a direct current dynamometer with automatic control. All thermodynamic parameters, e.g. intake pressure and temperature, temperatures of oil and coolant were controlled and monitored with high accuracy. More detailed information on the test stand can be found in [25, 26].

Table 1: Specifications of the research engine. [26]

Parameter names	**Values**
Displaced volume	498.5 cm^3
Bore	84 mm
Stroke	90 mm
Connecting rod	165 mm
Compression ratio	11.7
Number of valves	2
Fuel injector	Single stream, side mounted
Boost device	Vane compressor, electrically driven

Table 2: Specifications of the accelerometers. [27]

Manufacturer	PCB PIEZOTRONICS	
Type	PCB ICP M338A34	
Sensitivity	11.1	mV/g
Measurement range	$\pm$ 4905	m/s^2
Frequency range ($\pm$ 5%)	1-2000	Hz
Frequency range ($\pm$ 10%)	0.7-3000	Hz
Resonance frequency	$>$ 12	kHz
Wideband sensitivity	$\pm$ 0.2	m/s^2
Cross sensitivity	$<$ 5	$\%$
Impact resistance	$\pm$ 19620	m/s^2pk
Operating temperature	-54 $\rightarrow$ +121	°C
Temperature coefficient	$<$ 0.09	$\%/°C$
Stress sensitivity	$<$ 0.005	g/ε

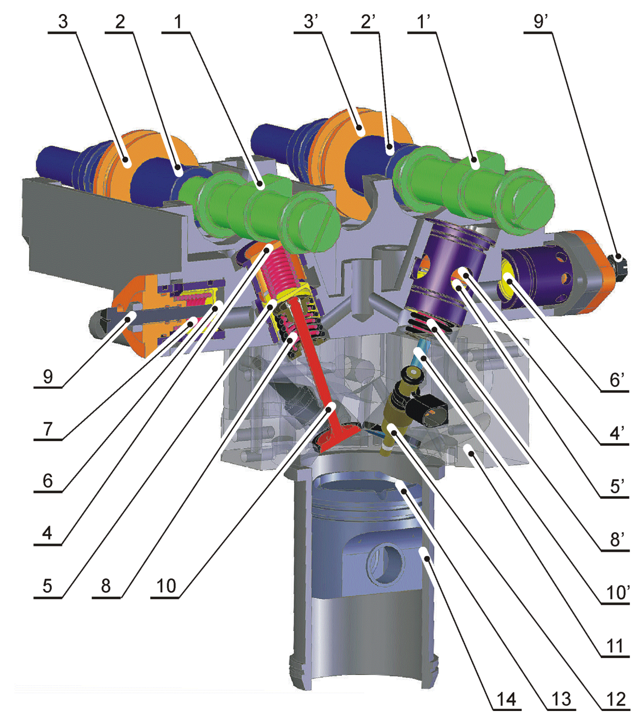

Figure 1: Cross-section of the research engine SB 3.5; 1) camshaft, 2) drive shaft, 3) sliding sleeve, 4) cam piston, 5) valve piston, 6) hydraulic accumulator piston, 7) hydraulic accumulator spring, 8) valve springs, 9) valve lift regulating screw, 10) valve, 11) engine head, 12) fuel injector, 13) piston, 14) cylinder liner. [28]

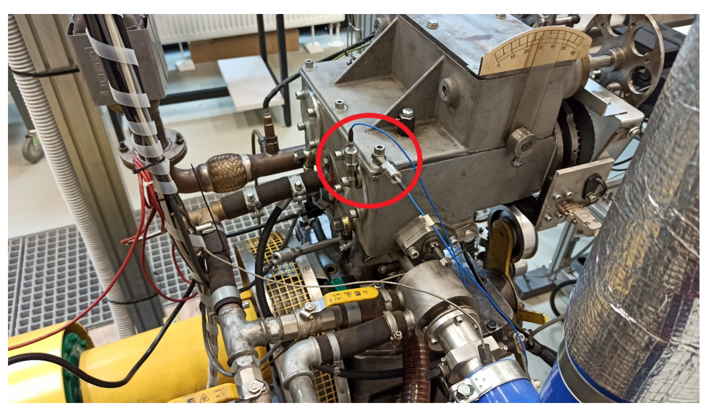

Figure 2: Location of accelerometers on the engine test bench (red circle).

METHODOLOGY

PRINCIPLES OF RADIAL BASIS FUNCTION NEURAL NETWORK Radial basis function neural network (RBFNN) is a feed forward network consisting of an input layer and a hidden layer interconnected to an output layer. This interconnection is a linear combination of the hidden layer signals [29]. The architecture of RBFNN is shown in Figure 3. Given an input vector $\mathbf{x}$, the network output y_k is expressed as follows [30]:

$$y_k(\mathbf{x}) = \sum_{j=1}^{n} w_{jk}\phi_j(\|\mathbf{x}-\mathbf{c}_j\|) + w_{0k} \tag{1}$$

where n is the number of neurons in the hidden layer, $\mathbf{c}_j$ is the vector determining the center of the basis function ϕ_j, w_{jk} are the final layer weights and w_{0k} is the bias term. The term $\|\mathbf{x}-\mathbf{c}_j\|$ indicates the Euclidean distance from vector $\mathbf{x}$ to the center $\mathbf{c}_j$. There are several basis functions that can be used, such as multi-quadratic, inverse multi-quadratic, thin plate spline, cubic or linear [30], but in this work, the Gaussian function, which is the most popular function for RBF, is used. The Gaussian function can be expressed as follows:

$$\phi(\|\mathbf{x}-\mathbf{c}_j\|) = \exp\left(-\frac{\|\mathbf{x}-\mathbf{c}_j\|^2}{\sigma^2}\right) \tag{2}$$

in which σ is called the spreading parameter. Increasing σ results in smoother approximation. However, too large σ would require a larger number of neurons to adapt to fast changing functions [21]. Advantages of RBFNN are its nonlinear mapping and generalization ability. Additionally, it is fast in learning and convergence [31].

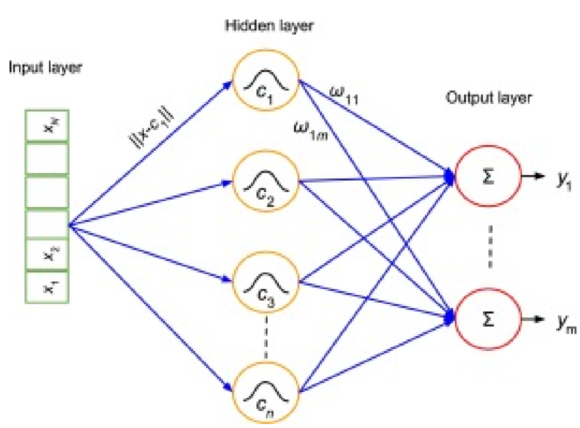

Figure 3: Architecture of a RBFNN. [32]

PRINCIPLES OF GENERALIZED REGRESSION NEURAL NETWORK Generalized regression neural network (GRNN) belongs to radial basis networks and is suitable for function approximation and model identification. GRNN consists of input layer, pattern layer (radial basis layer), summation layer and output layer, as depicted in Figure 4.

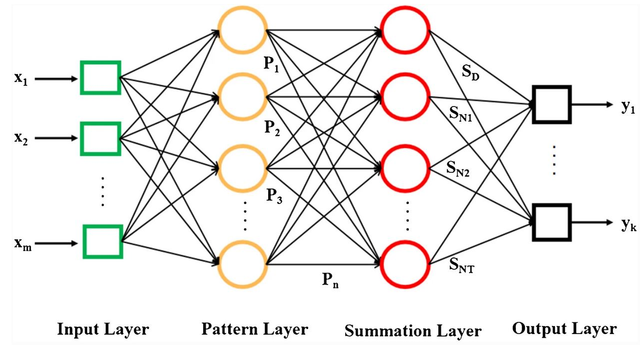

Figure 4: Architecture of the generalized regression neural network. [33]

The pattern layer operates similarly as the hidden layer in RBFNN. The output of the pattern layer pass through the summation layer, which calculates the weighted sum of the signals (for details see [34, 35]). The result is a mapping between the hidden layers and the output layer. Similarly to RBFNN, GRNN also has a strong nonlinear mapping ability. In addition to that, it has a fast learning speed and strong approximation ability. Other advantages of GRNN are its simple network architecture and robustness [33]. However, the major advantage of GRNN is its ability to provide good prediction with small data sets [34].

DATA PRE-PROCESSING AND ANALYSIS

VIBRATION AND CYLINDER PRESSURE CORRELATION The vibration signal is able to capture the events taking place during the engine operation. These events are for example intake valve opening or closing, piston slap and start of combustion, and can be detected as drastic changes in the amplitude in vibration signal [21]. It should be noted that the valve opening and closing heavily influenced the vibration signal, which is more severe compared to commercial engines. This issue is a result of unoptimized design of the research engine valvetrain. Fortunately, there are no significant mechanical interference during the combustion event. In Figure 5 the cylinder pressure with the corresponding vibration signal is presented.

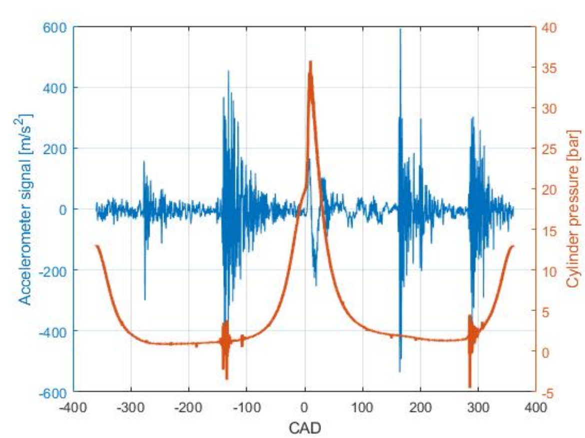

Figure 5: Vibration signal and cylinder pressure (OP 13: 2095 RPM)

Figure 6 presents the normalized vibration with respect to normalized cylinder pressure and its derivative, where correlation between the signals is clear. According to [36] comparing the derivative of cylinder pressure against the vibration signal as shown in Figure 6b is more informative than comparison between the vibration and pressure signals, as shown in Figure 6a.

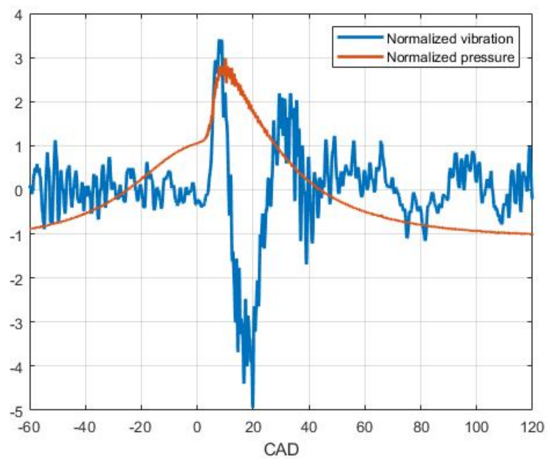

(a) Normalized vibration signal and cylinder pressure

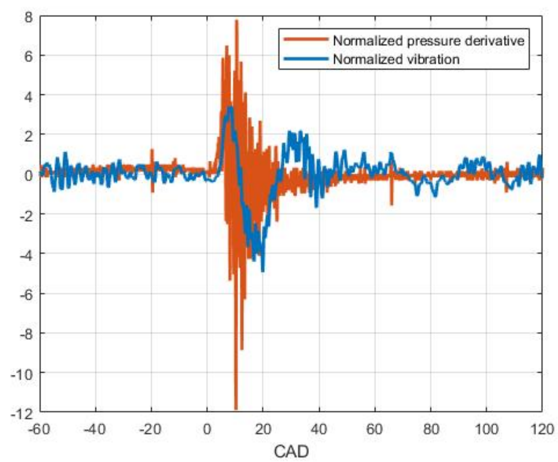

(b) Normalized vibration signal and cylinder pressure derivative

Figure 6: Normalized vibration and cylinder pressure signal (OP 13: 2095 RPM). The normalization presents the z-score of the signals with center 0 and standard deviation 1. There is a distinct correlation between the vibration and cylinder pressure during the combustion event.

It can be concluded that force impulses created by changes in the cylinder pressure are propagated throughout the engine block and are hence detected by the accelerometers.

Additionally, correlation between cylinder pressure and vibration signal can be measured with different signal analysis techniques such as the magnitude squared coherence estimate, fast Fourier transform (FFT) or power spectral density (PSD) [8, 36–38]. Combustion metrics, such as peak cylinder pressure or combustion phasing, can be calculated from the vibration signal as shown in [36]. Zero-crossing of the vibration signal is used to calculate peak cylinder pressure. Time delay between the cylinder pressure and vibration signal was obtained by observing the vibration and the first derivative of the cylinder pressure. In addition to that, [36] compared the first derivative of the rate of heat release to the vibration in order to estimate the parameters, such as combustion phasing and main injection. [38] and [37] used FFT as a feature extractor to detect and extract most dominant frequencies and their respective amplitudes. These features were then used to detect abnormal behaviour, such as misfire occurring during the combustion.

In this work, data analysis is focused more on the inspection of the data. Thus, the only pre-processing procedure performed on the vibration data has been data trimming around the combustion event.

CYLINDER PRESSURE PEGGING In-cylinder pressure is instrumental for this study as it provides reference and verification data. The recorded relative pressure traces for individual cycles were pegged to provide absolute values. To this end, the absolute pressure signal from the intake port was used as a reference value to correct in-cylinder pressure around the point, where valve flow was stagnated. The pegging procedure was applied to each separate engine cycle.

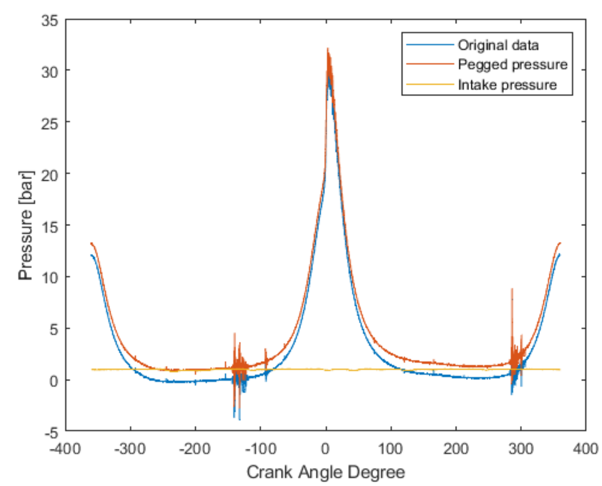

Figure 7: Example of the pegging process for the cylinder pressure.

IMPLEMENTATION AND RESULTS

The goal in this paper is to build a radial basis neural network model, valid for wide range of operating conditions. Two different series of data were used for virtual sensor development. The first data series consists of medium-low load operating points, namely **X60xx**, presented in Table A1. The second data series consists of operating points in a wider load range from low to high loads, namely **X43xx**, which is presented in Table A2.

RESULTS OF X60XX SERIES Initially, a RBFNN model was trained with this medium-low load data series, which consists of two operating points, marked as X6021 and X6027 respectively. The data was collected from 1000 consecutive cycles for each point with resolution of 0.1 CAD, in which 700 cycles were used as training data. The remaining 300 cycles were used for validation. Hence, there are 1400 cycles of data for training and 600 cycles for validation. Figure 8 presents the measured accelerometer signals and cylinder pressures of the two operating points averaged over 300 cycles. Additionally, the accelerometer signal and cylinder pressure are trimmed from -40 CAD to 40 CAD to concentrate on the combustion phase. This reduces the computation time, while preserving all relevant correlation between vibration and cylinder pressure signals.

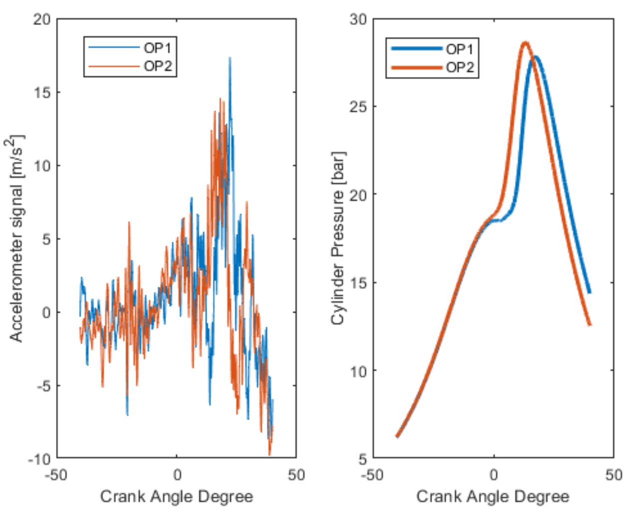

Figure 8: Accelerometer signals and cylinder pressures of the two operating points.

The model was trained using the *newrb* function from Deep Learning toolbox in MATLAB. There are two important parameters, which require tuning: the maximum number of neurons in the hidden layer and the spread of radial basis functions σ. These two parameters are tuned such that the mean square error loss is minimized with the minimum number of neurons. Figure 9 presents the network performance, in terms of mean square error (MSE), as function of the maximum number of neurons and the spreading parameter σ. As the test indicates, the most suitable maximum number of neurons is 75 and σ should be 3000. These values are implemented for the RBFNN training throughout this paper and all the prediction from this model will be denoted as **ANN75**.

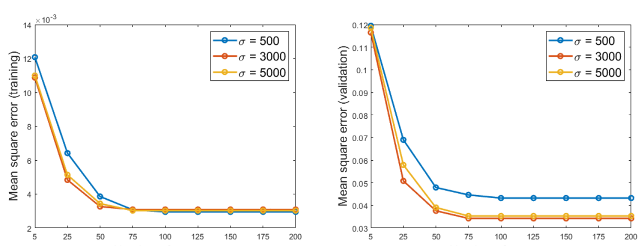

(a) Training (b) Validation

Figure 9: RBFNN performance as a function of maximum number of neurons and σ

Validation was carried out in two ways: by cycle-to-cycle and by the mean value of the 300 validating cycles. In the first part of validation, prediction is executed with the average of vibration and pressure data over the 300 validating cycles for each operating point. The predicted cylinder pressure of both operating points are compared to the averaged experimental cylinder pressure in Figure 10. The results show a good prediction with very small root mean square error (RMSE). Furthermore, the prediction was executed with every cycle in the validation data set and the goodness of fit in terms of RMSE is shown in Figure 11. The average RMSE for both operating points are low and it indicates good prediction of the pressure over the cycles with error being below 2 bar, except for few cycles, where the error is high for both operating points.

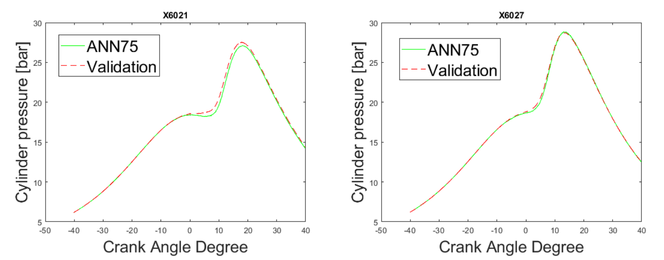

(a) X6021: RMSE = 0.29 bar (b) X6027: RMSE = 0.11 bar

Figure 10: Measured (red) and predicted pressure (green) at X6021 and X6027

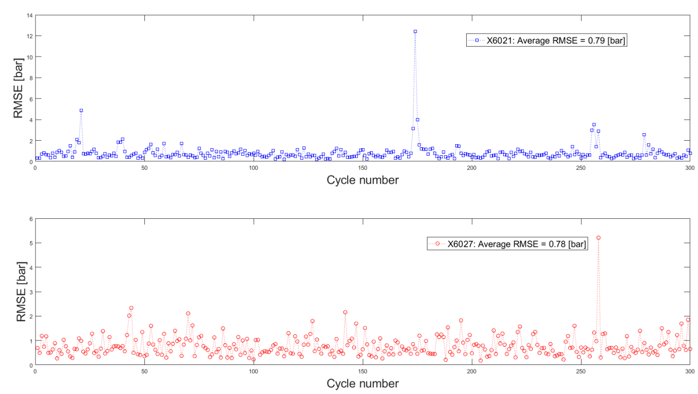

Figure 11: RMSE over the validation cycles.

Combustion parameters, such as peak cylinder pressure and peak pressure location are also investigated for both operating points. In Figure 12 and Figure 13 the predicted peak pressure values and locations errors are computed against the measured values for both X6021 and X6027 over the 300 cycles of validation data. The root mean square error in peak pressure values is kept at less than 2 bars. The peak pressure location errors are approximately at 1-2 CAD for both operating points.

In both operating points, the majority of 300 validating cycles has very small estimation error. However, due to some irregular cycles, in which there are defects such as misfiring, incomplete or late combustion, errors are unexpectedly high at these cycles. For example, in Figure 11, it can be seen some minor cycles, where the errors are excessively high. The similar result can also be seen in Figure 12 and Figure 13, where there are some irregular cycles with relatively high errors.

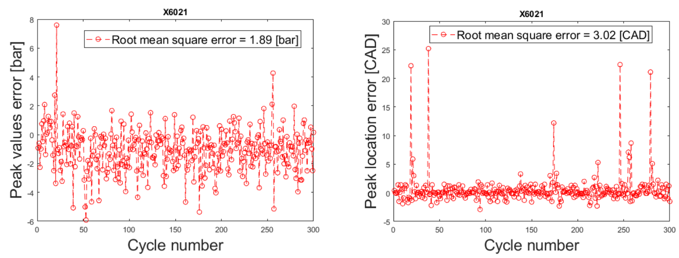

(a) Peak pressure

(b) Peak pressure location

Figure 12: Peak pressure comparison over validation cycles at X6021

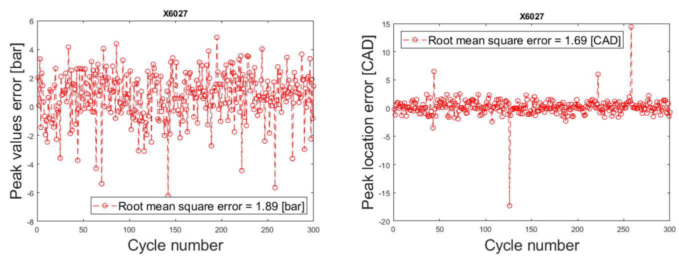

(a) Peak pressure

(b) Peak pressure location

Figure 13: Peak pressure comparison over validation cycles at X6027

RESULTS OF X43XX SERIES The approach was further applied to another series of engine data which consists of wider load range, from low loads to high loads, according to the specification of this test engine. The data consists of 27 operating points with 100 consecutive cycles for each point with resolution of 0.1 CAD. Detailed operating conditions are presented in Table A2. The data set was divided into 70 cycles for training and 30 cycles for validating. The training and validation cycles were chosen randomly. Figure 14 presents an example of 10 cycles of the training data from operating point 1 (OP1) in which indicated mean effective pressure (IMEP) is 4.497 bar.

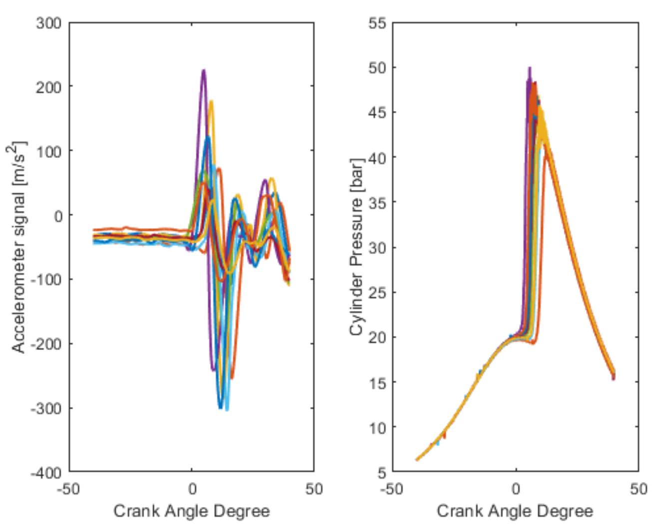

Figure 14: Example of 10 cycles of training data from OP1.

The RBFNN model was trained again with this set of training data and validated on all the cycles of the validating data set. Figure 15 shows the average RMSE over the cycles of the validation data at every operating point. As can be seen from the graph, the fitting results are deteriorated at several first operating points, where the loads are high. Otherwise, after operating point number 10 towards the end, the prediction errors are reasonably low and those points are corresponding to the low load conditions. Moreover, Figure 16 shows the fitting results at the first validation cycle of OP1 and OP3. The RMSE are 1.32 bar and 3.34 bar respectively. It appears from the results that the radial basis function neural network model has difficulties to reconstruct the cylinder pressure from a high load condition, in which the pressure rises rapidly and fluctuates at the peak. As can be seen from the plots, the two pressure curves are very steep and narrow.

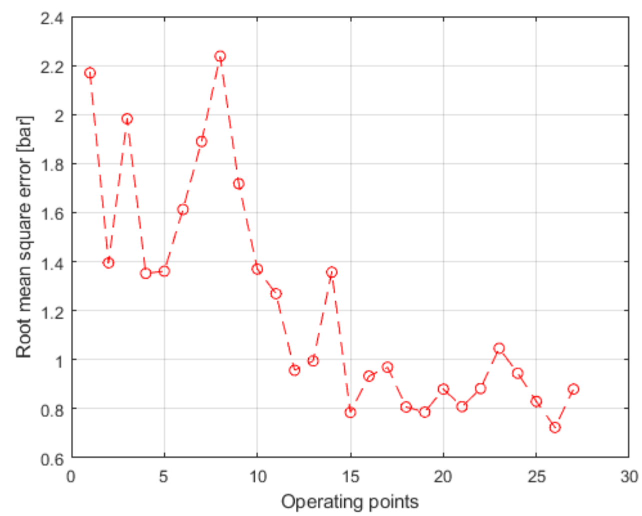

Figure 15: Average RMSE over 30 cycles of 27 operating points with RBFNN.

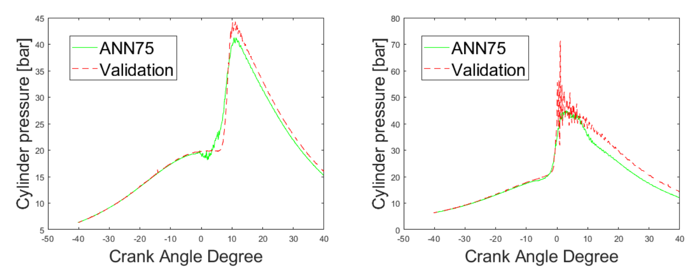

(a) OP1: IMEP = 4.497 bar

(b) OP3: IMEP = 3.969 bar

Figure 16: Prediction results at OP 1 and OP 3 using RBFNN

In order to tackle the challenge at high load conditions, the generalized regression neural network model was implemented. Performance analysis of both GRNN and RBFNN has been conducted at the end of this section. The GRNN model was trained by using the Deep Learning toolbox in MATLAB with the command *newgrnn* and one hyperparameter that requires tuning is the spreading parameter σ. In order to fit a smoother function, σ can be chosen as large value, but small values are selected to fit the data closely. In this work, the spreading parameter σ was selected by a network performance test in which σ that makes the mean square error minimized will be selected. Figure 17 indicates that the suitable spreading parameter should be 125. The number of neurons in the pattern and summation layer are chosen by the function based on the value of the σ. This chosen value of σ created pattern layer with 1890 neurons and a summation layer of 801 neurons. Fitting result in terms

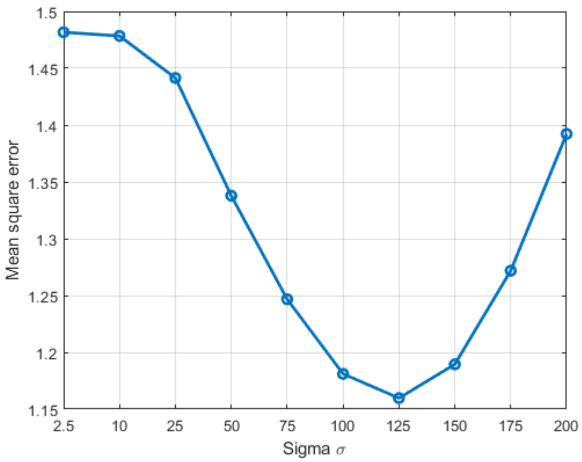

Figure 17: GRNN performance as a function of σ.

of RMSE is shown in Figure 18, where it presents the average RMSE over the 30 cycles of validating data of the whole 27 operating points. The average errors over the validating cycles are kept relatively small, i.e., under 2 bar. Similar to the performance of the RBFNN, prediction error is higher at the high load conditions and it becomes smaller at the low load operating points. However, the amplitude of the prediction error by GRNN is relatively lower. In every operating point, the error is approximately 30 % less than the error by using RBFNN, as shown in Figure 15. In Figure 19, the first validation cycles of OP1 and OP3 are also verified with the GRNN model. It shows a much better fit compare to the RBFNN with mean square errors of 0.36 bar and 0.91 bar respectively.

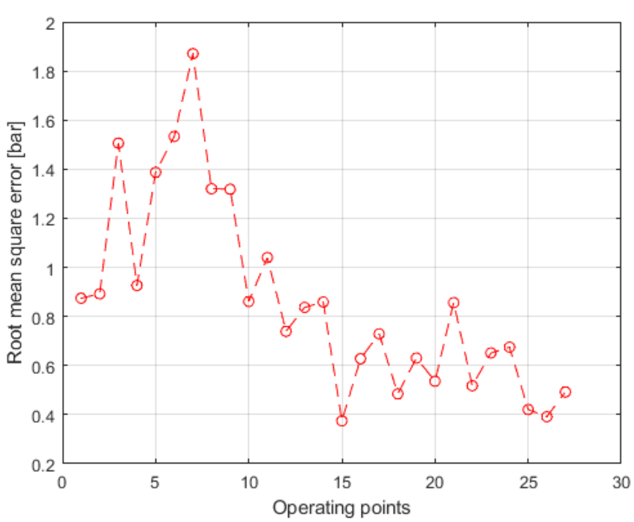

Figure 18: Average RMSE over 30 cycles of 27 operating points with GRNN.

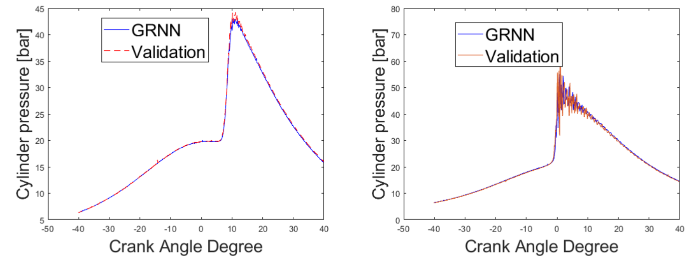

(a) OP1: IMEP = 4.497 bar (b) OP3: IMEP = 3.969 bar

Figure 19: Prediction results at OP1 and OP3 using GRNN

In addition to the in-cylinder pressure, other combustion parameters were also taken into account during the validating phase, such as peak pressure, peak pressure location and location of 50 % mass fraction burned (MFB50). The average root mean square errors of each operating point of the peak cylinder pressure and peak location in crank angle degree are shown in Figure 20 and Figure 21 respectively. Performance of both RBFNN and GRNN models are exhibited. Due to the fluctuation around the top dead center, the RMSE of estimation for peak pressure value was kept under 0.8 bar with GRNN and 1.1 bar with RBFNN. The two models have similar trends of result in the peak pressure location, but GRNN definitely has smaller error in both high and low load regions. Errors are relatively small except for a few points where there are some abnormal cycles in the validation data, which makes the errors become 3-4 CAD.

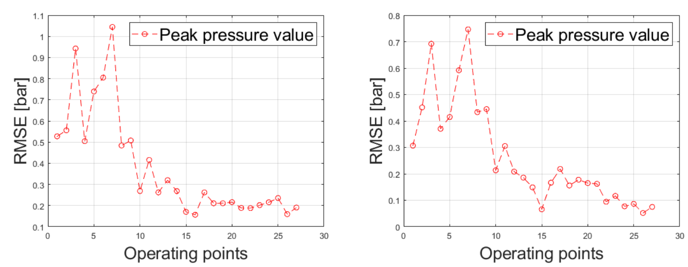

(a) RBFNN (b) GRNN

Figure 20: Prediction results of peak pressure values by RBFNN and GRNN

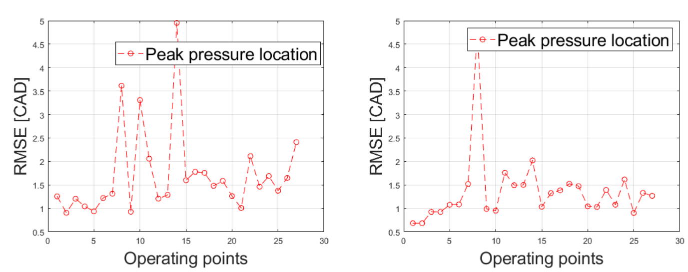

(a) RBFNN (b) GRNN

Figure 21: Prediction results of peak pressure location by RBFNN and GRNN

The reconstructed cylinder pressure was used to calculate the location of MFB50. The procedure starts with calculating heat release rate with respect to crank angle $\frac{dQ}{d\theta}$ by using Equation

3 [39], in which p, V are the cylinder pressure and volume respectively. The ratio of specific heat γ is kept constant at 1.4 in this work.

$$\frac{dQ}{d\theta} = \frac{\gamma}{\gamma - 1} p \frac{dV}{d\theta} + \frac{1}{\gamma - 1} V \frac{dp}{d\theta} \tag{3}$$

The cumulative heat release is then calculated by a cumulative sum of dQ. Location of MFB50 is determined by finding the crank angle where the corresponding cumulative heat release is closest to 50 % of the maximum cumulative heat release. Results of MFB50 are compared to the measured values in Figure 22. The graph indicates that a majority of operating points have low error, approximately only from 0.5 CAD to 1.0 CAD. However, there are a few points of which the errors are higher, also due to abnormal cycles in the validating data set. Figure 23 shows some exemplary abnormal cycles with misfiring, incomplete or late combustion, extracted from the validating data set. These two cycles belong to operating point 8 (OP8) and operating point 10 (OP10), which show high errors in the previous analysis.

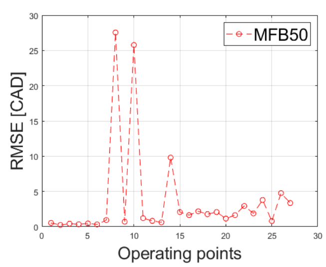

(a) RBFNN

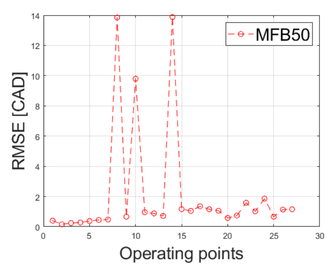

(b) GRNN

Figure 22: Prediction results of CA50 location by RBFNN and GRNN

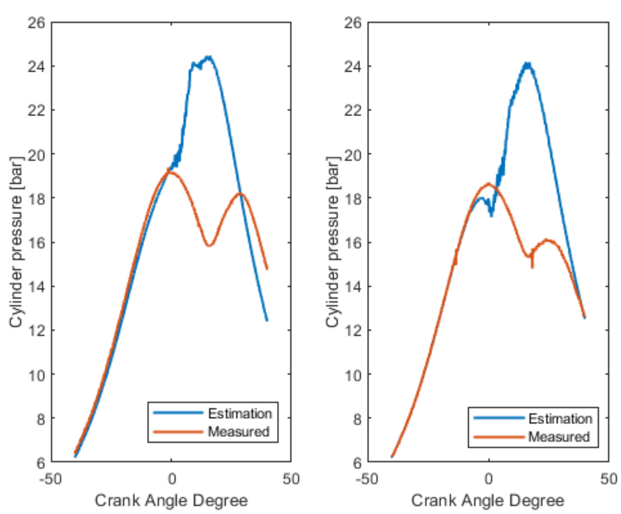

Figure 23: Example of 2 abnormal cycles of validating data from OP8 and OP10.

Finally, the fitting results of several operating points are shown in Figures 24, 25, 26 and 27. The average of vibration signal over 30 cycles of validating data was used as the input to reconstruct the pressure curves. The predicted pressure curves are compared with the average of cylinder pressure over 30 cycles of validating data. The first and the second plots present the prediction results by GRNN and RBFNN at high load conditions. The third and the fourth plot show results of the two network models at low load conditions.

In the high load cases, GRNN model captures the rapid rise of the pressure curve very well while the RBFNN is not as successful. There are always some offset between the measurement and the prediction by RBFNN, specially in the expansion phase. Both models performed well under low load conditions. Nevertheless, it can be seen that in a same operating point, RBFNN tends to have slightly higher error than GRNN.

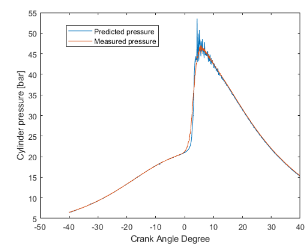

(a) OP 2

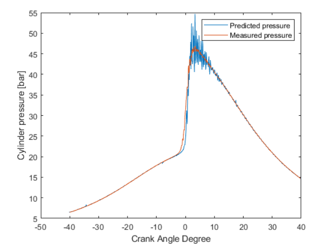

(b) OP 3

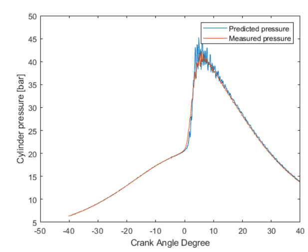

(c) OP 5

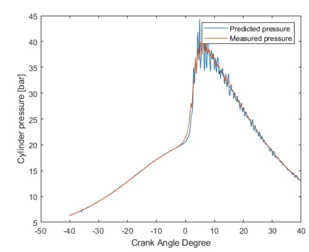

(d) OP 7

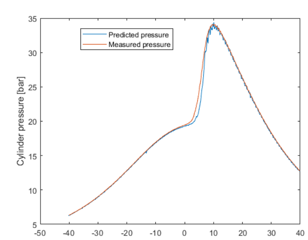

(e) OP 11

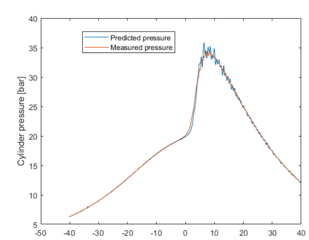

(f) OP 13

Figure 24: Measured and predicted cylinder pressure of high load engine conditions by GRNN

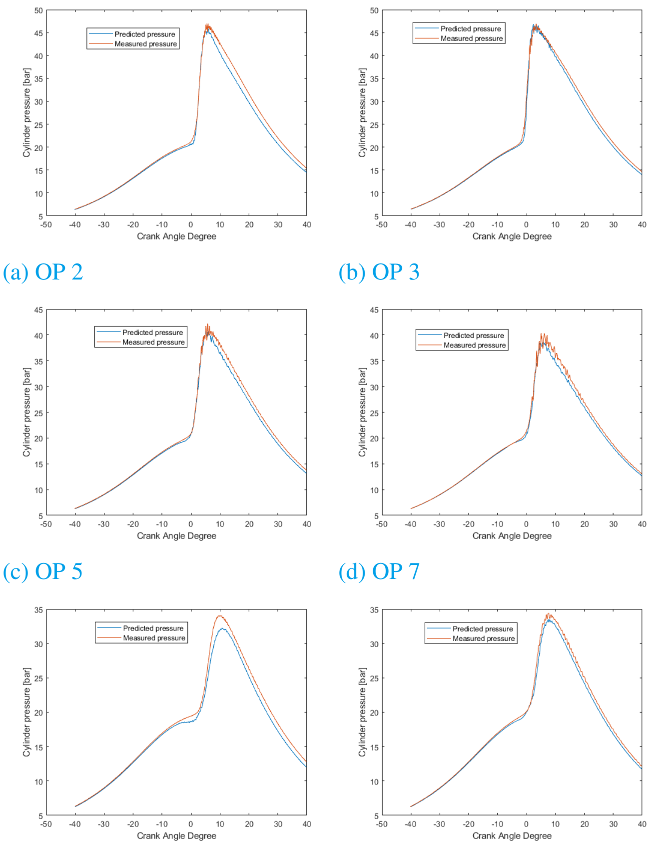

(a) OP 2 (b) OP 3

(c) OP 5 (d) OP 7

(e) OP 11 (f) OP 13

Figure 25: Measured and predicted cylinder pressure of high load engine conditions by RBFNN

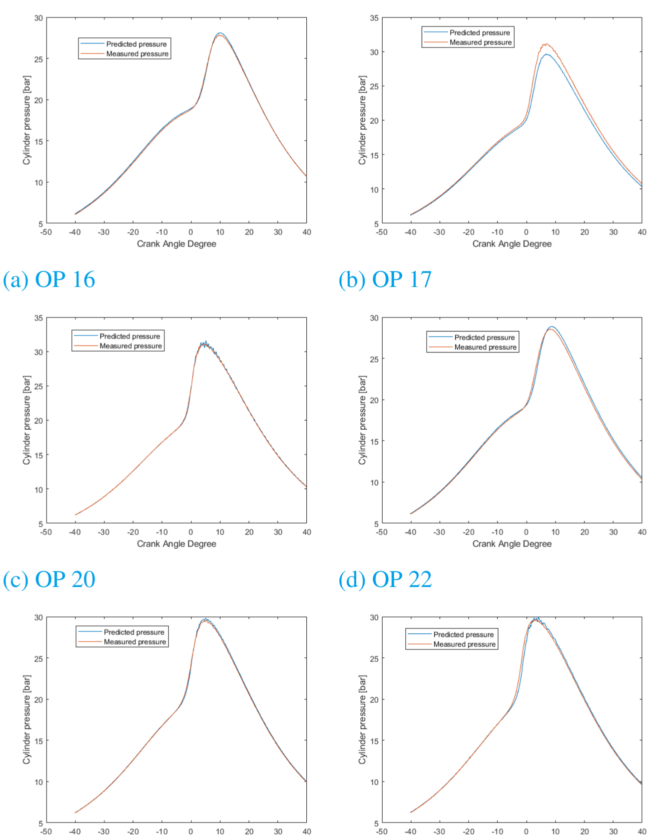

(a) OP 16 (b) OP 17

(c) OP 20 (d) OP 22

(e) OP 25 (f) OP 27

Figure 26: Measured and predicted cylinder pressure of low load engine conditions by GRNN

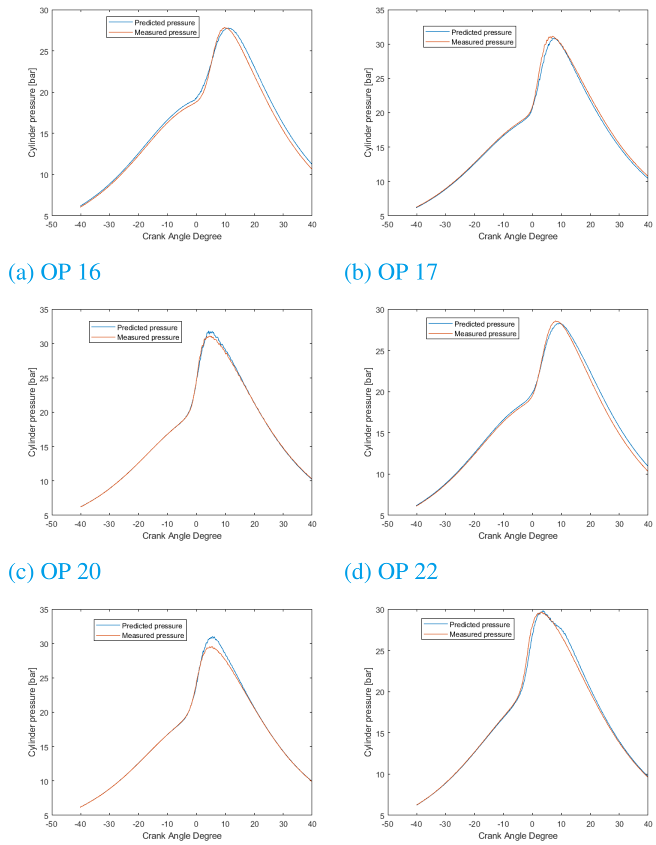

(a) OP 16 (b) OP 17

(c) OP 20 (d) OP 22

(e) OP 25 (f) OP 27

Figure 27: Measured and predicted cylinder pressure of low load engine conditions by RBFNN

CONCLUSIONS

In this work, two neural network models were built to reconstruct cylinder pressure from vibration signal. Accelerometers were installed on the surface of the engine cylinder head and their measurements were used to estimate cylinder pressure utilizing a radial basis function neural network and a generalized regression neural network. The pressure prediction was validated and sensitivity analysis was carried out in terms of combustion parameters, such as peak pressure and combustion timing.

Moreover, in high load conditions of HCCI combustion, the generalized regression network performed better compared to the radial basis network. This can be explained by the slight difference in the last layer of the generalized regression network, which is the extra normalized dot product function right before the linear function of the output layer. It helps the function approximation deal with the fast changing function like the pressure curve in the high load HCCI combustion. The fact that in high-load combustion, GRNN performs better than RBFNN is an open question and is currently being investigated.

The results have shown that vibration signal carries sufficient information to estimate combustion parameters independently of the engine platform or combustion concept.

REFERENCES

[1] J. Yan, R. Rogalla, and T. Kramer, "Diesel combustion and transient emissions optimization using taguchi methods," *SAE Transactions*, pp. 755–768, 1993.

[2] K. Schten, G. Ripley, A. Punater, and C. Erickson, "Design of an automotive grade controller for in-cylinder pressure based engine control development," tech. rep., SAE Technical Paper, 2007.

[3] T. Schnorbus, S. Pischinger, T. Körfer, M. Lamping, D. Tomazic, and M. Tatur, "Diesel combustion control with closed-loop control of the injection strategy," tech. rep., SAE Technical Paper, 2008.

[4] S. Kimura, O. Aoki, Y. Kitahara, and E. Aiyoshizawa, "Ultra-clean combustion technology combining a low-temperature and premixed combustion concept for meeting future emission standards," *Sae Transactions*, pp. 239–246, 2001.

[5] C. Bohn, O. Magnor, and M. Schultalbers, "State observer based analysis of crankshaft speed measurements with application to misfire detection," in *2005 International Conference on Control and Automation*, vol. 1, pp. 239–244, IEEE, 2005.

[6] G. Panzani, F. Östman, and C. H. Onder, "Engine knock margin estimation using in-cylinder pressure measurements," *IEEE/ASME transactions on Mechatronics*, vol. 22, no. 1, pp. 301–311, 2016.

[7] Y. Gao and R. Randall, "Reconstruction of diesel engine cylinder pressure using a time domain smoothing technique," *Mechanical systems and signal processing*, vol. 13, no. 5, pp. 709–722, 1999.

[8] R. Han, C. Bohn, and G. Bauer, "Recursive engine in-cylinder pressure estimation using kalman filter and structural vibration signal," *IFAC-PapersOnLine*, vol. 51, no. 31, pp. 700–705, 2018.

[9] R. Han, C. Bohn, and G. Bauer, "Recursive engine in-cylinder pressure estimation merely using structural vibration signal," in *2020 European Control Conference (ECC)*, pp. 240–245, IEEE, 2020.

[10] R. Johnsson, "Cylinder pressure reconstruction based on complex radial basis function networks from vibration and speed signals," *Mechanical systems and signal processing*, vol. 20, no. 8, pp. 1923–1940, 2006.

[11] V. Zurita and A. Ågren, "A new approach of the combustion process in diesel engines using vibration measurements. part 1: Reconstruction of cylinder pressure from vibration measurements," *International Journal of Acoustics and Vibration*, vol. 8, no. 4, 2003.

[12] J. Hunicz and D. Piernikarski, "Investigation of combustion in a gasoline engine using spectrophotometric methods," in *Optoelectronic and Electronic Sensors IV*, vol. 4516, pp. 307–314, International Society for Optics and Photonics, 2001.

[13] G. Dong, Y. Chen, Z. Wu, L. Li, and R. Dibble, "Study on the phase relation between ion current signal and combustion phase in an hcci combustion engine," *Proceedings of the Combustion Institute*, vol. 35, no. 3, pp. 3097–3105, 2015.

[14] J. Hunicz, P. Filipek, and A. Sobiesiak, "Application of ion current measurement to identification of combustion parameters in a homogeneous charge compression ignition engine," *Metrology and Measurement Systems*, vol. 25, no. 1, 2018.

[15] F. Taglialatela, N. Cesario, M. Porto, S. Merola, P. Sementa, and B. Vaglieco, "Use of accelerometers for spark advance control of si engines," *SAE International Journal of Engines*, vol. 2, no. 1, pp. 971–981, 2009.

[16] O. Chiavola, G. Chiatti, L. Arnone, and S. Manelli, "Combustion characterization in diesel engine via block vibration analysis," tech. rep., SAE Technical Paper, 2010.

[17] C. Bennett, *Reconstruction of gasoline engine in-cylinder pressures using recurrent neural networks*. PhD thesis, University of Sussex Brighton, UK, 2014.

[18] A. Businaro, N. Cavina, E. Corti, G. Mancini, D. Moro, F. Ponti, and V. Ravaglioli, "Accelerometer based methodology for combustion parameters estimation," *Energy Procedia*, vol. 81, pp. 950–959, 2015.

[19] G. Chiatti, O. Chiavola, E. Recco, A. Magno, E. Mancaruso, and B. M. Vaglieco, "Accelerometer measurement for mfb evaluation in multi-cylinder diesel engine," *Energy*, vol. 133, pp. 843–850, 2017.

[20] J. C. Peña and G. Zurita, "Vibration based reconstruction of the cylinder pressure in diesel engines by using neural networks," *Revista Investigación & Desarrollo*, vol. 1, no. 5, 2005.

[21] K. Bizon, G. Continillo, E. Mancaruso, and B. M. Vaglieco, "Reconstruction of in-cylinder pressure in a diesel engine from vibration signal using a rbf neural network model," tech. rep., SAE Technical Paper, 2011.

[22] V. M. Janakiraman, X. Nguyen, and D. Assanis, "Nonlinear identification of a gasoline hcci engine using neural networks coupled with principal component analysis," *Applied Soft Computing*, vol. 13, no. 5, pp. 2375–2389, 2013.

[23] H. Bendu, B. Deepak, and S. Murugan, "Application of grnn for the prediction of performance and exhaust emissions in hcci engine using ethanol," *Energy conversion and management*, vol. 122, pp. 165–173, 2016.

[24] J. Hunicz, M. Mikulski, M. S. Geca, and A. Rybak, "An applicable approach to mitigate pressure rise rate in an hcci engine with negative valve overlap," *Applied Energy*, vol. 257, p. 114018, 2020.

[25] J. Hunicz and P. Kordos, "Experimental study of the gasoline engine operated in spark ignition and controlled auto-ignition combustion modes," tech. rep., SAE Technical Paper, 2009.

[26] J. Hunicz, M. Mikulski, G. Koszałka, and P. Ignaciuk, "Detailed analysis of combustion stability in a spark-assisted compression ignition engine under nearly stoichiometric and heavy egr conditions," *Applied Energy*, vol. 280, p. 115955, 2020.

[27] PCB Piezotronics, "Sensors to measure vibration, acoustics, force, pressure, load, strain, shock and torque." `https://www.pcb.com`, 2022. [Online; accessed 14-April-2022].

[28] J. Hunicz and M. Mikulski, "Investigation of the thermal effects of fuel injection into retained residuals in hcci engine," *Applied Energy*, vol. 228, pp. 1966–1984, 2018.

[29] D. S. Broomhead and D. Lowe, "Radial basis functions, multi-variable functional interpolation and adaptive networks," tech. rep., Royal Signals and Radar Establishment Malvern (United Kingdom), 1988.

[30] C. Harpham and C. W. Dawson, "The effect of different basis functions on a radial basis function network for time series prediction: A comparative study," *Neurocomputing*, vol. 69, no. 16-18, pp. 2161–2170, 2006.

[31] G. A. Montazer, D. Giveki, M. Karami, and H. Rastegar, "Radial basis function neural networks: A review," *Computer Reviews Journal*, vol. 1, no. 1, pp. 52–74, 2018.

[32] H. Faris, I. Aljarah, and S. Mirjalili, "Chapter 28 - evolving radial basis function networks using moth–flame optimizer," in *Handbook of Neural Computation* (P. Samui, S. Sekhar, and V. E. Balas, eds.), pp. 537–550, Academic Press, 2017.

[33] S. Liu, H. Zhang, B. Wang, S. Dai, Y. Yang, and G. Gan, "Generalized regression neural network-based prediction methods for overlying strata failure zone height," *Arabian Journal of Geosciences*, vol. 14, p. 2547, Nov 2021.

[34] D. Specht, "A general regression neural network," *IEEE Transactions on Neural Networks*, vol. 2, no. 6, pp. 568–576, 1991.

[35] M. H. Beale, M. T. Hagan, and H. B. Demuth, "Neural network toolbox user's guide," *The MathWorks*, pp. 77–81, 2010.

[36] A. Businaro, N. Cavina, E. Corti, G. Mancini, D. Moro, F. Ponti, and V. Ravaglioli, "Accelerometer based methodology for combustion parameters estimation," *Energy Procedia*, vol. 81, pp. 950–959, 2015. 69th Conference of the Italian Thermal Engineering Association, ATI 2014.

[37] K. Jafarian, M. Mobin, R. Jafari-Marandi, and E. Rabiei, "Misfire and valve clearance faults detection in the combustion engines based on a multi-sensor vibration signal monitoring," *Measurement*, vol. 128, pp. 527–536, 2018.

[38] J. L. Firmino, J. M. Neto, A. G. Oliveira, J. C. Silva, K. V. Mishina, and M. C. Rodrigues, "Misfire detection of an internal combustion engine based on vibration and acoustic analysis," *Journal of the Brazilian Society of Mechanical Sciences and Engineering*, vol. 43, p. 336, Jun 2021.

[39] J. B. Heywood, *Internal combustion engine fundamentals*. McGraw-Hill Education, 2018.

CONTACT INFORMATION

Hoang Nguyen Khac
hoang.kh.nguyen@aalto.fi

Department of Electrical Engineering and Automation, Aalto University
Maarintie 8, 02150, Espoo, Finland

ACKNOWLEDGEMENT

This research is part of the Clean Propulsion Technologies -project (CPT) funded by Business Finland.

The experimental data were obtained as a part of the Lublin University of Technology statutory research, contract No. FD-20/IM-5/44.

DEFINITIONS/ABBREVIATIONS

Abbreviations

CAD	Crank angle degree
FFT	Fast Fourier transform
GR	Generalized regression
GRNN	Generalized regression neural network
HCCI	Homogeneous charge compression ignition
IMEP	Indicated mean effective pressure
MFB50	50 % mass fraction burned
MSE	Mean square error
PSD	Power spectral density
RBF	Radial basis function
RBFNN	Radial basis function neural network
RMSE	Root mean square error

Symbols

w_k	weight
w_{0k}	bias
y_k	output of the neural network
ϕ	basis function
σ	spreading parameter
$\mathbf{c}$	vector determining the center of the basis function
$\mathbf{x}$	input vector of the neural network
n	number of neurons in the hidden layer

APPENDIX

Table A1: Engine Operating Conditions of the **X60xx** data series. Each operating point contains 1000 cycles.

	Speed [rpm]	IMEP [bar]	Lambda	EGR [%]	Pmax [bar]
X6021	1500	3.468	1.042	37.51	28.863
X6027	1500	2.786	1.101	46.98	27.86

Table A2: Engine Operating Conditions of the **X43xx** data series. Each operating point contains 100 cycles.

	Speed [rpm]	IMEP [bar]	Lambda	EGR [%]	Pmax [bar]
OP 1	917	4.497	1.014	33.8	43.82
OP 2	1110	4.358	1.018	34.5	46.392
OP 3	1308	3.969	1.023	36.3	46.206
OP 4	1506	3.756	1.029	38.9	40.665
OP 5	1700	3.527	1.016	38.9	40.665
OP 6	1899	3.402	1.036	42.4	39.404
OP 7	2096	3.219	1.022	44.5	39.33
OP 8	1110	3.778	1.096	37.9	35.328
OP 9	1308	3.436	1.1	43.4	34.959
OP 10	1506	3.131	1.104	44.7	28.85
OP 11	1703	2.986	1.102	47.9	33.625
OP 12	1899	2.771	1.101	48.7	33.823
OP 13	2095	2.707	1.107	49.0	34.48
OP 14	2291	2.627	1.165	49.5	31.35
OP 15	1300	2.127	1.253	55.6	28.875
OP 16	1509	2.228	1.275	55.3	27.929
OP 17	1705	2.217	1.255	54.7	30.895
OP 18	1901	2.193	1.232	54.4	31.141
OP 19	2097	2.162	1.253	55.8	31.796
OP 20	2291	1.947	1.265	58.3	30.857
OP 21	1110	2.464	1.249	50.4	29.143
OP 22	1309	2.08	1.239	56.7	28.658
OP 23	1508	2.038	1.235	58.0	27.773
OP 24	1705	1.875	1.248	60.4	29.539
OP 25	1903	1.829	1.247	60.7	29.437
OP 26	2098	1.702	1.266	62.0	29.659
OP 27	2293	1.611	1.288	63.2	29.44